

The string spectrum from large Wilson loops

Pushan Majumdar *
Max-Planck-Institut für Physik,
Föhringer Ring 6, D-80805 München, Germany.

22 November 2002
MPI-PhT/2002-70

Abstract

We look at energies of the low lying states of the hadronic string in three dimensional SU(2) lattice gauge theory by forming correlation matrices among different sources. We are able to go to previously inaccessible time separations. This is made possible by using a new algorithm proposed by Lüscher and Weisz which lets us measure the exponentially small values of large Wilson loops with sufficient accuracy.

1 Introduction

The mechanism of quark confinement in Quantum Chromodynamics remains unsolved to this date. One of the most appealing pictures of confinement is that in the QCD vacuum, flux tubes are formed between quarks and anti-quarks giving rise to a linearly rising potential.

There have been several attempts [1] to write down effective theories for these flux tubes also known as hadronic strings. For a recent review see [2]. Typically in all these theories, the potential is represented as a series in r (the quark anti-quark separation) with σr as the leading term at large r . The coefficient σ of this linear term is called the string tension. The sub-leading

*email: pushan@mppmu.mpg.de

terms go as inverse powers of r . One of the most striking features of these theories has been the prediction of a universal coefficient of the $1/r$ term [3]. This coefficient, commonly denoted as c , has the value $-\frac{\pi}{24}(d-2)$ where d is the number of space-time dimensions. Several studies have looked at features of the string [4] [5] and, in particular, the ground state and the coefficient c [6] are known quite well. However controversy still exists regarding the excited states and the predicted energy differences of integral multiples of π/r . A recent study by Caselle *et al.* [7] looks at the string picture in Ising gauge theories using powerful numerical techniques which uses the dual symmetry of the model. However for non-Abelian gauge theories, such precise numerical techniques are lacking. To circumvent this problem, studies by Juge *et al.* [8] [9] ¹ on Yang-Mills theories have relied on asymmetric lattices.

A recent algorithm suggested by Lüscher and Weisz [10] go a long way to remedy this problem as it allows us to measure small expectation values with good accuracy even for theories with continuous gauge symmetries. For a discussion of the algorithm and optimization issues relevant for Wilson loops we refer the reader to [11]. Recently this algorithm has been used to look at string breaking [12], static 3-quark potential [13] and correlation between pairs of Wilson loops [14]. Here we use this algorithm to measure the low lying states of the hadronic string in pure Yang-Mills lattice gauge theory.

We would like to point out that this study is only exploratory in nature. Therefore we have concentrated more on measurements at larger time separations using the Lüscher - Weisz algorithm rather than using sophisticated wave functions. A complete study will probably require both. Due to computational and time constraints we were unable to undertake such a study at the moment, but hope to do so in the future.

Section II is devoted to setting the notation and a discussion of lattice preliminaries. In section III we look at the classification of the string states. Section IV is devoted to some of the simulation details. In particular we set the scale on the lattice and discuss the smearing scheme in this section. In section V we present our results on the spectrum and discuss different procedures to extract the energy of the states. Section VI deals looks at the energy differences at different β values, and finally in section VII we draw our conclusions. In the appendix we present a discussion of our error analysis.

¹We thank the referee for pointing out this reference.

All our figures, unless explicitly stated, are in lattice units.

2 Preliminaries

We will work in 2+1 dimensions with SU(2) lattice gauge theory and the Wilson action. We also impose the usual periodic boundary conditions. The fundamental degrees of freedom of this theory are the SU(2) matrices associated to the links of the lattice which we denote by U . The action is defined on the smallest closed paths on the lattice called plaquettes. Our partition function is given by

$$Z = \int_{U \in SU(2)} \mathcal{D}U e^{\frac{\beta}{2} \sum_p \text{tr}(U_p)} \quad (1)$$

where the sum is over all plaquettes p and U_p is the directed product of U 's around the plaquette. To make a connection to the continuum theory we have to identify β with $4/g^2$ and take both g and the lattice spacing to zero. The choice of Wilson action is also important for us as this action allows the construction of a positive transfer matrix [17]. Both the algorithm that we use, and the physical interpretation of what we do, rely on the existence of such a transfer matrix.

The transfer matrix of a model provides the relation between the functional integral and the Hamiltonian formalism. Let us call links in the space direction as U_s and in the time direction as U_t . In the temporal gauge where all the time like links $U_t(t+1, t)$ are set to $\mathbf{1}$, it is easy to interpret the transfer matrix as connecting states in one time slice to the next. The states on which this transfer matrix acts are square integrable wave functions $\Psi[U_s]$. The space of these wave functions form a Hilbert space.

The partition function Z in the presence of external test charges can be written in terms of the transfer matrix as

$$Z_{\bar{q}q} = \text{tr}(\mathbb{P}_{\bar{q}q} \mathcal{T}^n)$$

where $\mathbb{P}_{\bar{q}q}$ is the projection onto the relevant sub-space of the Hilbert space. For a more complete discussion of the transfer matrix formalism see [18].

The main observable that we are concerned with is the Wilson loop. In

the continuum, the Wilson loop is given by

$$W(C) = \text{tr } \mathbf{P} \left(\exp \left(\int_C A_\mu dx_\mu \right) \right) \quad (2)$$

where C is any closed curve and \mathbf{P} denotes path ordering. On the lattice the Wilson loop is defined by

$$W(C) = \frac{1}{m} \text{tr} \left\{ \prod_{l \in C} U_l \right\} \quad (3)$$

where again C is a closed curve and m is the dimension of the matrix U .

Wilson loops of extent (R, T) can be interpreted in the transfer matrix formalism, as the correlation of sources between points separated by a distance R , propagating for time T . Thus it is possible to look at correlations between string states by choosing appropriate $\Psi[U_s]$ as sources for the Wilson loops in Yang-Mills theory.

The other observable that we look at is the Polyakov loop. It is defined by

$$P(\vec{x}, T) = \text{tr } \mathbf{T} \left(\exp \left(\int_0^T A_0(\vec{x}, t) dt \right) \right) \quad (4)$$

where T is the extent of the lattice in the time direction and \mathbf{T} denotes time ordering. On the lattice the Polyakov loop is defined by

$$P(\vec{x}, T) = \text{tr} \left\{ \prod_{l=0}^{T-1} [U_l(\vec{x})] \right\}. \quad (5)$$

The Polyakov measures the excess free energy of the vacuum induced by a static test quark.

3 String states

The states of the hadronic string that we want to look at carry different quantum numbers. Therefore it is important to classify them. Here we briefly outline the classification scheme.

The string states that we are interested in, are configurations at fixed time with both ends of the string fixed so that only transverse degrees of freedom

are left. In analogy to [15], an effective Hamiltonian for the transverse degrees of freedom for a string of length r can be written as

$$\mathcal{H} = \frac{\pi}{2r^2} \int_0^r d\kappa \left(\frac{\mathcal{P}_i^2(\kappa)}{\sigma} + \sigma x_i'^2(\kappa) \right) \quad (6)$$

where x' is derivative of x with respect to κ and \mathcal{P} are the canonical momenta. σ , with dimensions of $(length)^{-2}$, is the string tension and i goes over the transverse degrees of freedom. Let $\kappa \in [0, r]$ be the coordinate along the string. Then the configuration and transverse momenta of the string can be represented as

$$x_i(\kappa) = \sum_{n=1}^{\infty} x_i^n \sin\left(\frac{n\pi\kappa}{r}\right), \quad (7)$$

$$\mathcal{P}_i(\kappa) = \sum_{n=1}^{\infty} \mathcal{P}_i^n \sin\left(\frac{n\pi\kappa}{r}\right). \quad (8)$$

The Hamiltonian is now given by

$$\mathcal{H} = \frac{\pi}{4r} \sum_{n=1}^{\infty} \left[\frac{(\mathcal{P}_i^n)^2}{\sigma} + n^2 \sigma (x_i^n)^2 \right]. \quad (9)$$

To go to the number operator basis, let us now define the creation and annihilation operators such that

$$x_i^n = \frac{1}{\sqrt{n\sigma}} (a_i^{\dagger n} + a_i^n) \text{ and } \mathcal{P}_i^n = i\sqrt{n\sigma} (a_i^{\dagger n} - a_i^n), \quad (10)$$

with $[a_i^{\dagger n}, a_j^m] = \delta_{ij} \delta^{nm}$. In terms of the creation and annihilation operators, the Hamiltonian can be formally written as

$$\mathcal{H} = \sum_{n=1}^{\infty} \frac{n\pi}{r} (a_i^{\dagger n} a_i^n + \frac{(d-2)}{2}). \quad (11)$$

In this expression, the second term is divergent and we use zeta function regularisation for it. Using $\zeta(-1) = -\frac{1}{12}$, we can rewrite the Hamiltonian as

$$\mathcal{H} = \left(\sum_{n=1}^{\infty} \frac{n\pi}{r} a_i^{\dagger n} a_i^n \right) - \frac{\pi}{24r} (d-2) \quad (12)$$

where d is the number of space-time dimensions. Thus from the zero point energy we obtain the universal $1/r$ contribution to the potential at large r . For a similar derivation see [16]. From equation (12), we read off the energy difference between successive states to be π/r . These are two very important predictions of the string picture and we will confront both of them with our data.

In 2+1 dimensions, we have only one set of oscillators since there is only one transverse dimension and the eigenstates of the Hamiltonian fall under four different channels distinguished by their behaviour under the discrete transformations of parity and charge conjugation. In contrast, in 3+1 dimensions there are two transverse directions and hence two independent sets of oscillators. This brings in an additional angular momentum quantum number given the usual 2-d harmonic oscillator algebra.

We will look at 2+1 dimensions and there, since we have only one transverse direction, we drop the index i . To classify our states, we now determine the behaviour of a^n and $a^{\dagger n}$ under parity and charge conjugation. For this it is sufficient to note that parity implies $x(\kappa) \rightarrow -x(\kappa)$ and charge conjugation takes $x(\kappa) \rightarrow x(\pi - \kappa)$. From this definition it is easy to see that under parity $\{a^n, a^{\dagger n}\} \rightarrow \{-a^n, -a^{\dagger n}\}$ and under charge conjugation $\{a^n, a^{\dagger n}\} \rightarrow \{(-1)^{n+1}a^n, (-1)^{n+1}a^{\dagger n}\}$. Below we list the first few string states along with their C and P quantum numbers.

++	+-	--	-+
$ 0\rangle$	$a_1^\dagger 0\rangle$	$a_2^\dagger 0\rangle$	$a_2^\dagger a_1^\dagger 0\rangle$
$(a_1^\dagger)^2 0\rangle$	$(a_1^\dagger)^3 0\rangle$ $a_3^\dagger 0\rangle$	$(a_1^\dagger)^2 a_2^\dagger 0\rangle$ $a_4^\dagger 0\rangle$	$(a_1^\dagger)^3 a_2^\dagger 0\rangle$ $a_1^\dagger a_4^\dagger 0\rangle$ $a_2^\dagger a_3^\dagger 0\rangle$
$(a_1^\dagger)^4 0\rangle$ $a_1^\dagger a_3^\dagger 0\rangle$ $(a_2^\dagger)^2 0\rangle$			

Here we will look at the ground states in each channel as well as the first excited state in the $\{++\}$ channel.

Polyakov Loop			Wilson Loop (all β values)						
β	5	7.5	10	T	2	4	6	8	12
iupd	1600	1600	3200	iupd	100	200	300	400	600

Table 1: Parameters used in the algorithm.

4 Simulation Details

In this work we perform three different kinds of simulations. First we measure Polyakov loop correlation functions. Apart from giving accurate information about the ground state, this also helps us set the scale on the lattice. Secondly, to look at the ground states in various channels, we perform simulations with sources belonging to different channels. Finally to investigate excited states in the same channel we use sources of the same shape but create correlation matrices by using different smearing parameters. An outline of these procedures is given below.

Most of our calculations are carried out at $\beta = 5$ on a 24^3 lattice. However we also perform some measurements at larger β and lattice volume.

4.1 Parameters of the algorithm

We work with three couplings viz. $\beta = 5, 7.5$ and 10 . The lattice volumes are $24^3, 36^3$ and 48^3 respectively. At $\beta = 5$, we also measure Polyakov loops on a lattice of extent 24 in the space direction but 8 in the time direction.

For our simulations we use the Lüscher-Weisz multi-level algorithm. Since this algorithm is relatively new, we list some of the parameters that we use with this algorithm. We restrict ourselves to one level of averaging and estimate the average of the product of two 2-link operators over a number of sub-lattice updates ². (At $\beta = 10$ we use a product of four 2-link operators instead of two). For each sweep of heat-bath we use three sweeps of over-relaxation. In table 1 we list the number of sub-lattice updates (iupd) we use for various quantities.

At $\beta = 5$ these values are close to optimal. For the Polyakov loops at $\beta = 7.5$, the optimal value for the number of sub-lattice updates is probably

²For a definition of these terms see [10]

more than what we used. $\beta = 10$ required a different averaging scheme. We had to use a product of four 2-link operators instead of two to obtain the kind of error reduction as at the lower values of β .

4.2 Setting the scale

We use the string tension to set the scale on the lattice. To obtain the string tension, we begin by measuring the Polyakov loop correlation functions for various separations. The Polyakov loop correlator, at a distance r can be represented as

$$\langle P(r, T)P(0, T) \rangle = \sum_{i=0}^{\infty} b_i \exp[-V_i(r)T] \quad (13)$$

where b_i 's are integers [6]. At large r where the string picture is thought to be valid, $V(r) = V_0(r)$ is given by $\sigma r + \tilde{V} + c/r + \dots$ where \tilde{V} is a constant depending only on β , σ is the string tension, c is the universal constant mentioned above and the dots represent terms with higher inverse powers of r . In three dimensions $c = -\pi/24$.

From correlation functions, we obtain the potential $V_0(r)$ by

$$V(r) = - \lim_{T \rightarrow \infty} \frac{1}{T} \log \langle P(r, T)P(0, T) \rangle \quad (14)$$

Then we define the force $F(r)$ by the symmetric difference of the potential i.e. $F(r) = [V(r+1) - V(r-1)]/2$. We also compute c at every value of r by defining $c(r) = [V(r+1) + V(r-1) - 2V(r)]r^3/2$. These are tabulated in table 2. To obtain the string tension, we plot $F(r)$ against $1/r^2$ in Fig. 1. Then the intercept gives us the value of the string tension ($a^2\sigma$) and the asymptotic value of the slope gives us the constant c .

The only problem with the above analysis is that the string behaviour is expected only at large distances and since time and computational resources prevent us from going to too large distances, the quantities determined from the plots have a significant admixture of short distance effects. Therefore it is preferable to use the locally determined $c(r)$'s for as large r 's as possible to set the slope and then determine the intercept to get the string tension. For the 24^3 lattice we were able to use $c(r)$ to set the slope. However for the other two cases $c(r)$ was not sufficiently accurately determined to be of use.

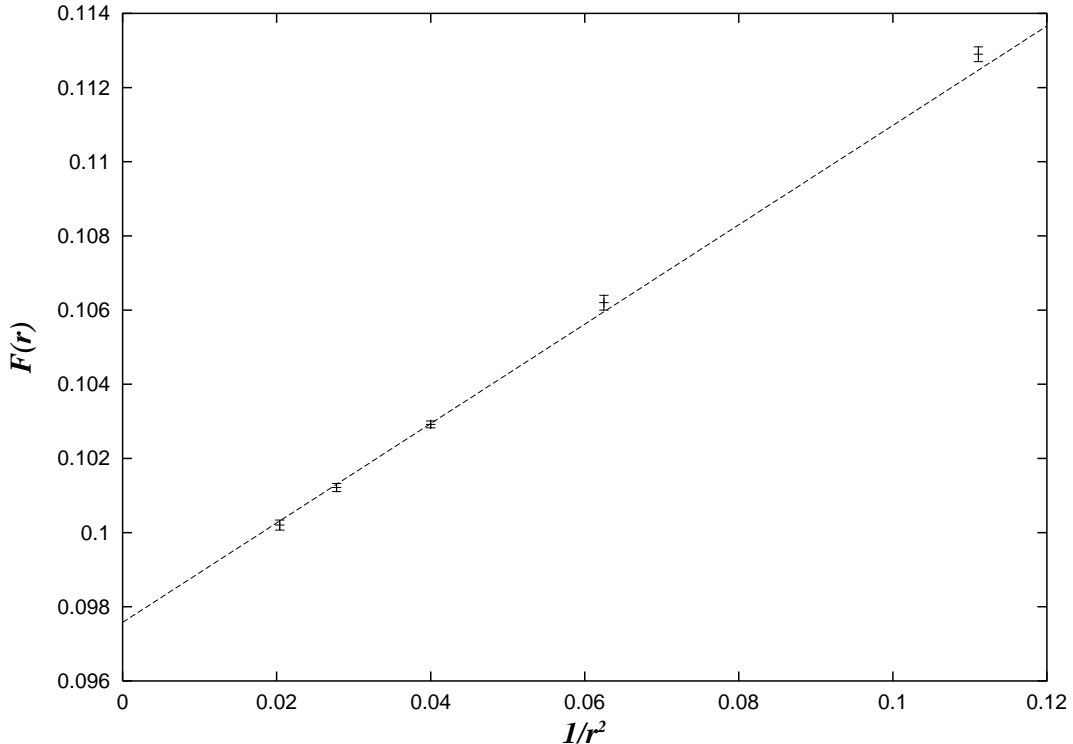


Fig. 1. The force $F(r)$ extracted from the Polyakov loop vs $1/r^2$ for lattice size 24^3 . $\beta = 5$.

In those cases both the parameters were obtained from the graph. In table 3 we tabulate $a\sqrt{\sigma}$ and the Sommer scale r_0 [19] defined by $r_0^2 F(r_0) = 1.65$. In the table we quote $\sqrt{\sigma} r_0$. The scale can be set explicitly in different ways, for example, we use $\sqrt{\sigma} = (0.5 \text{ fm})^{-1}$.

At $\beta = 5$, our result for $a\sqrt{\sigma}$ compares nicely with Teper's [20] value of 0.3129 (20). We also look at how $c(r)$ compares with what we obtain from perturbation theory. From the two loop static quark potential $V(r)$ in [21] we obtain the perturbative value of $c(r)$ at $\beta = 5$ as

$$c(r) = \frac{r^3}{2} \frac{\partial^2 V(r)}{\partial r^2} = -\frac{3r}{4\pi\beta} = -\frac{3r}{20\pi} \quad (15)$$

In Fig. 2 we plot this perturbative value along with the values of $c(r)$ given in table 3. This figure shows the transition from perturbative to non-

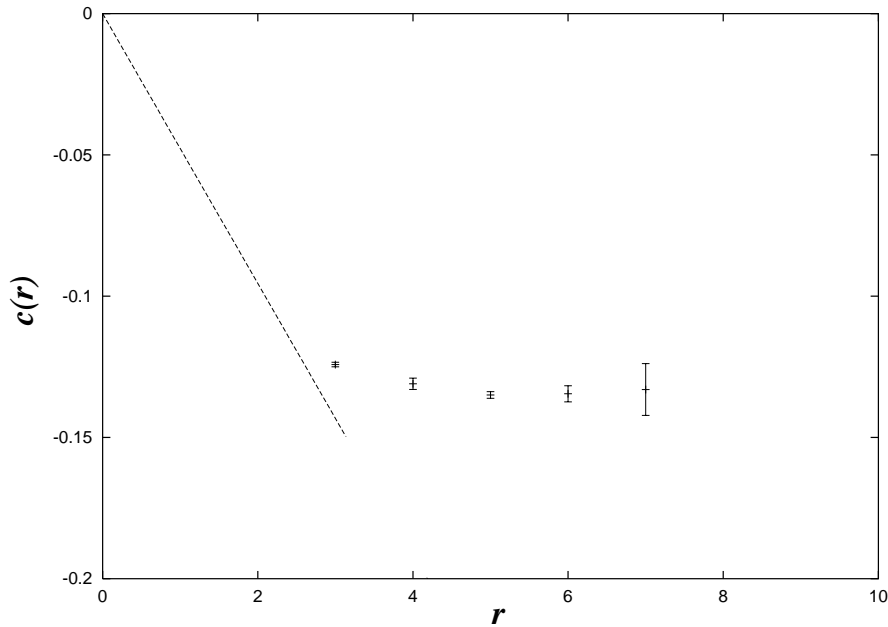


Fig. 2. $c(r)$ at $\beta = 5$. The curve is 2 loop perturbation theory.

perturbative behaviour for c . This is interesting because although the short distance behaviour depends on the gauge theory, the long distance string picture gives the same value for all gauge theories. For similar results in $SU(3)$, see [6].

4.3 Correlation matrices

The advantage of the Wilson loop is that it also offers the possibility to study the higher excited states. This can be done by using sources which couple preferentially to the required state. If the optimal sources are unknown, this can be achieved by forming correlation matrices $C(r, T)$ among various wave functions. Upon diagonalisation, the linear combination of the wave functions which give the eigenvectors of $C(r, T)$ are the required sources. The matrix element $C_{ij}(r, T)$ is nothing but a Wilson loop of extent T in

the time direction, with $source_i$ at one end and $source_j$ at the other. The sources are paths between points separated by distance r .

To explore the four different channels, we use a basis of four paths shown in Fig. 3. where the staples are of length $\lfloor r/2 \rfloor$.

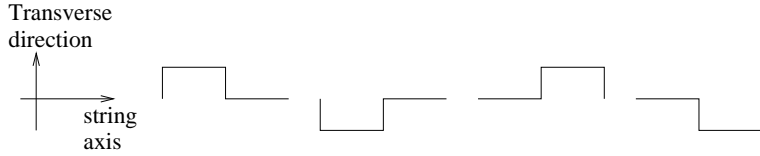


Fig. 3. The basis elements of the correlation matrix.

These paths can be combined into orthogonal channels invariant under the action of C and P as shown in Fig. 4.

CP

$$\begin{aligned}
 ++ &= \left(\begin{array}{c} \text{[Step up]} + \text{[Step down]} + \text{[Step up]} + \text{[Step down]} \end{array} \right) \\
 +- &= \left(\begin{array}{c} \text{[Step up]} - \text{[Step down]} + \text{[Step up]} - \text{[Step down]} \end{array} \right) \\
 -- &= \left(\begin{array}{c} \text{[Step up]} - \text{[Step down]} - \text{[Step up]} + \text{[Step down]} \end{array} \right) \\
 -+ &= \left(\begin{array}{c} -\text{[Step up]} - \text{[Step down]} + \text{[Step up]} + \text{[Step down]} \end{array} \right)
 \end{aligned}$$

Fig. 4. The eigenstates of the correlation matrix.

To look at excited states in the $\{++\}$ channel, we take the straight path but create different sources by using different smearing parameters. Thus in this case our sources are defined as

$$source_i = \mathcal{P} \left(\prod_{k=1}^r (U + \gamma_i \sum S) \right) \quad (16)$$

where $\gamma_i \in \{0.1, 0.3, 0.5\}$ and \mathcal{P} denotes projection back to $SU(2)$. U is the original link and S are the space-like staples. This procedure can be applied

recursively and we do four levels of smearing. While this may not be an optimal choice for the sources, it was sufficient for our purposes. Another advantage of smearing is that it reduces fluctuation of the sources. So even when we use the different paths to probe the different channels, we use one level of smearing with $\gamma = 0.5$.

The eigenvalues of the correlation matrix, for large time separations, are related to the energies of the various states of the sources. We find that these matrices are always dominated by the ground state and that the higher excited states are suppressed by several orders of magnitude.

5 Results

5.1 Polyakov loops

From the Polyakov loop correlators, we get energies of the ground state and the first excited state. At $\beta = 5$, the ground state is obtained from a 24^3 lattice and the first excited state from a combination of 24^3 and 8×24^2 lattices.

The energy is given by equation (14). The corrections to the energies are due to finite volume and mixing with higher energy states. Both of these can be quite reliably estimated. First we look at the leading order finite volume correction. Neglecting the higher energy states, the measured energy of a state is

$$-\frac{1}{T} \log(\langle PP \rangle(r)) = V(r) - \frac{1}{T} \log(1 + e^{-(L-2r)(\sigma - c/r(L-r))T}). \quad (17)$$

Here $V(r)$ is an improved estimate of the energy and the second term is the finite volume correction. We will call the argument of the log $(1 + \mathcal{V}(r))$. L is the extent of the lattice in the space direction which here is 24.

Next we come to the correction due to the presence of higher energy states. We will compute the correction to the first excited state. There are two states which contribute to the second excited state of the Polyakov loop. They correspond to $a_1^\dagger{}^2|0\rangle$ and the $a_2^\dagger|0\rangle$. However we have explicit measurements for both these states. Thus our correction factor is given by

$$\mathcal{Q}(r, T) = e^{-TE_1^{++}(r)} + e^{-TE_0^{--}(r)}. \quad (18)$$

We estimate further higher order corrections to be smaller than our statistical errors.

The measured energy obtained from the 24^3 lattice is overwhelmingly dominated by the ground state with the finite volume effects and effects from the higher states being smaller than our statistical errors. In contrast the value measured from the 8×24^2 lattice contains a significant contribution from the first excited state. To extract this state we subtract the ground state contribution, as obtained from the 24^3 lattice, from the $\langle PP \rangle$ expectation value. From equations (17) and (18) we also expect finite volume effects and contamination due to higher excited states for $V(r)$ from the 8×24^2 lattice.

Taking all these into account, our formula for the first excited state from the Polyakov loop is given by

$$E_1(r) = -\frac{1}{8} \log \left(\frac{\langle PP \rangle(r)}{1 + \mathcal{V}(r)} - e^{-8E_0(r)} - \mathcal{Q}(r, 8) \right) \quad (19)$$

where \mathcal{V} is the leading order finite volume correction and \mathcal{Q} is the correction due to higher states. Our results are tabulated in table 4.

In the preceding analysis we have assumed that the coefficients b_0 and b_1 given in equation (13) are unity as predicted by the free theory. Agreement of the energies with the ones determined from the Wilson loops bears out this assumption. There are departures from the free theory predictions too. Free theory predicts $b_2 = 2$ which implies a degenerate E_1^{++} and E_0^{--} state. However explicit measurement shows that this degeneracy is lifted and these states occur separately with coefficients unity. Since the coefficients can only change by integers, any other value for all the four b 's is effectively ruled out.

5.2 Wilson Loops

We first use the Wilson loop to look at the ground states of the four different channels. In this case since we know the symmetries of the invariant subspaces under \mathbf{C} and \mathbf{P} , we directly take the appropriate combinations of the matrix elements to diagonalise the correlation matrix. The energies are obtained by taking the ratio of the eigenvalues at fixed r but different T 's. Thus they are given by

$$E = -\frac{1}{T_2 - T_1} \log \frac{\lambda(r, T_2)}{\lambda(r, T_1)} \quad (20)$$

where $T_2 > T_1$ and $\lambda(r, T)$ is an eigenvalue of the correlation matrix $C(r, T)$. This however is just a naive estimate of the energies. Actually there are contributions from the higher states. That is why it is desirable to choose as large a value of T as possible [22]. To try to take this into account let us expand λ 's as

$$\lambda(r, T) = \alpha_1 e^{-E_0(r)T} + \alpha_2 e^{-E_1(r)T} + \dots \quad (21)$$

where E_0 is the ground state in a given channel and E_1, E_2 etc. are the higher energy states in the same channel. We will estimate the correction to the ground state by taking into account the contribution only due to the next excited state. At a fixed value of r , let

$$\lambda(T_1) = \alpha_1 e^{-E_0 T_1} \left(1 + \frac{\alpha_2}{\alpha_1} e^{-\delta T_1} \right), \quad (22)$$

$$\lambda(T_2) = \alpha_1 e^{-E_0 T_2} \left(1 + \frac{\alpha_2}{\alpha_1} e^{-\delta T_2} \right) \quad (23)$$

where $\delta = (E_1 - E_0)$ to leading order. Then the correction to the energy is given by

$$-\frac{1}{T_2 - T_1} \log \frac{\lambda(T_2)}{\lambda(T_1)} = \bar{E} + \frac{1}{T_2 - T_1} \left[\frac{\alpha_2}{\alpha_1} e^{-\delta T_1} (1 - e^{-\delta(T_2 - T_1)}) \right]. \quad (24)$$

Here the left hand side of the equation is the measured energy and \bar{E} is the improved estimate. As seen from this expression the correction has an exponential dependence on T_1 and a linear dependence on $T_2 - T_1$. Both these trends are seen in the data.

We concentrate mostly on the 24^3 lattice at $\beta = 5$. On this lattice, we measure correlation matrices with T extent's of 2, 4, 6 and 8 respectively. We extract the energies by two procedures. The first one is to do a fit to the form $\alpha \exp(-Et)$. This gives a naive estimate and these results are tabulated in table 5. In the second case we compute the energy from the six different combinations of T_1 and T_2 and then fit it to the form given in equation (24) with \bar{E} , $\frac{\alpha_2}{\alpha_1}$ and δ as the fit parameters. However this requires accurate data for stable fits and we were only able to do this with confidence for the first two energy states. Our statistics for $T = 8$ was not good enough for the higher states. Nevertheless at $\beta = 5$, we were able to obtain an extrapolation for the third state using only the $T = 2, 4$ and 6 data. For the fourth state even that was not possible. All these values are given in table 6.

From the data we estimate that the error in replacing $\log(1 + \frac{\alpha_2}{\alpha_1} \exp(-\delta T_1))$ by $\frac{\alpha_2}{\alpha_1} \exp(-\delta T_1)$ in equation (24) is well below our statistical errors for the first two states. We also checked that \bar{E} was within our error bars even with a 20% change in the value of δ . The most stringent condition on the fits come from the value of α_2/α_1 . The maximal value of α_2/α_1 is the ratio of the degeneracy of the states between the level considered and the next level. Any data set which violated this criterion, was considered not accurate enough to do a stable extrapolation to infinite T and has not been used.

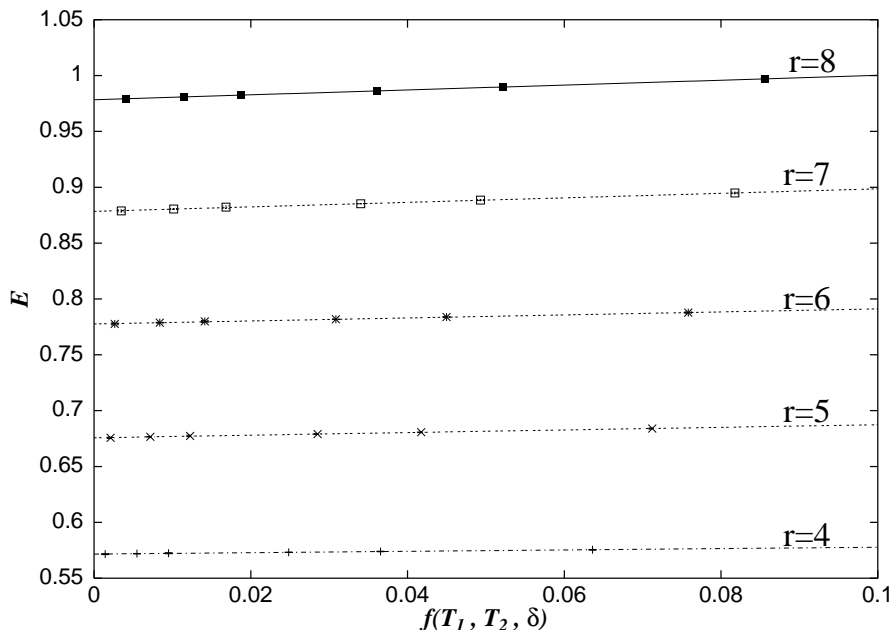


Fig. 5. Extrapolation of energies for ground state of $\{++\}$ channel. $\beta = 5$.

For the $\{++\}$ channel we have the explicit values for E_0^{++} and E_1^{++} . This information can be used to compute the second term in equation (24) with $\frac{\alpha_2}{\alpha_1}$ and \bar{E} as unknown parameters. The resulting data can be fitted to a form $ax + b$ to obtain \bar{E} and $\frac{\alpha_2}{\alpha_1}$. These values are shown against E_0^{++} in table 6. As seen from the data, the error bars here are much larger than the ones on E_0^{++} . This is because the estimated energy difference between the two states is not constant, but varies with varying T_1 and T_2 . We took the mean

value of this difference for δ . That is a good approximation for small r where the difference is small, but becomes worse as r increases. The uncertainty reported in the values of E_0^{*++} comes from the difference of the fitted values if one uses the extreme values of δ instead of the mean. In Fig. 5 we plot the extrapolations for the E_0^{*++} values.

In this plot the x-axis is the function $f(T_1, T_2, \delta)$ given by

$$f(T_1, T_2, \delta) = \frac{1}{T_2 - T_1} [e^{-\delta T_1} (1 - e^{-\delta(T_2 - T_1)})] \quad (25)$$

The symbols $+$, \times , $*$, \square and \blacksquare correspond to r values of 4,5,6,7 and 8 respectively. As seen from the plots, the slope of the fitted lines increase with increasing r .

To illustrate the importance of these corrections, we plot the energy difference between the ground state and excited states at $\beta = 5$ in Fig. 6. In

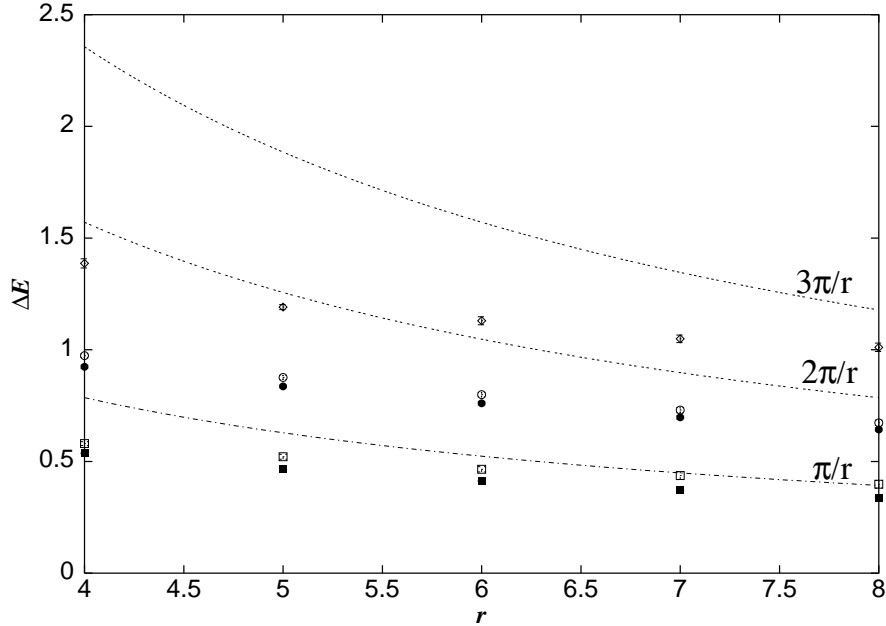


Fig. 6. Energy differences at $\beta = 5$. The open symbols are naive energy differences and the filled ones are the extrapolated ones.

this figure the open symbols \square , \circ and \diamond denote the naive energy differences

while filled symbols \blacksquare and \bullet are the ones obtained after performing the finite T corrections. The curves are the expected energy differences of π/r , $2\pi/r$ and $3\pi/r$. The uncorrected data set seems to contradict the string prediction as the energy difference between the ground state and the first excited state tends to become more than the string value at large r . However the corrected data shows no such trend but for large r seems to approach a value close to the one predicted by the string theory.

This behaviour persists even at higher values of β . In Fig. 7 we plot the energy difference between the first and the second states at $\beta = 10$. In

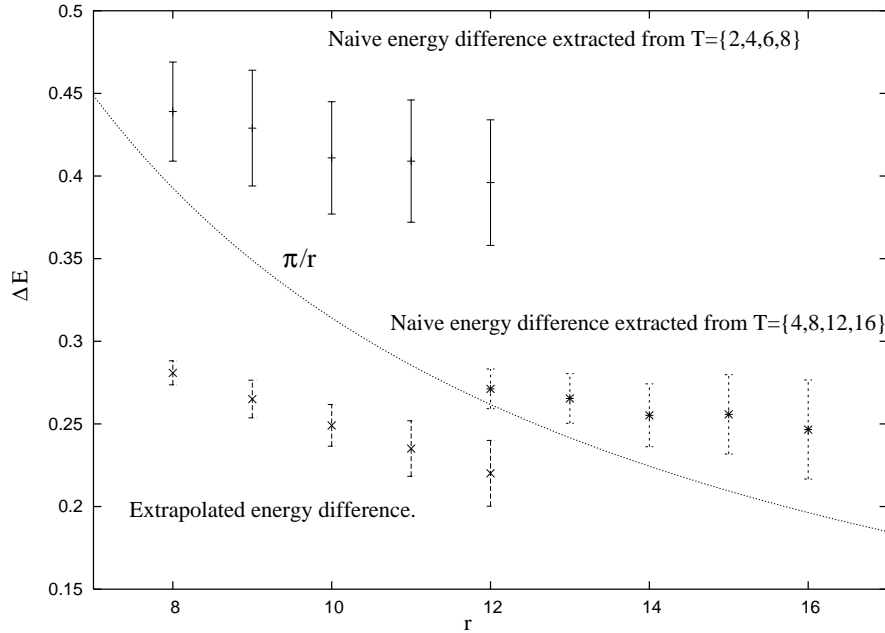


Fig. 7. Energy differences at $\beta = 10$. This figure illustrates how the naive energy difference changes depending on the time extent of the correlation matrices. The lowest set of points show the energy difference obtained by doing the extrapolation to $T = \infty$ as described in the text. The dotted curve is the π/r curve predicted by the free theory.

this figure the topmost set of points are the naive energy differences between the states E_0^{++} and E_0^{+-} . The lowest set of points are the energy differences

obtained by doing the extrapolation to $T = \infty$ using the same data set. Finally the set in the middle shows the naive energy difference between the same states, but now determined from the correlation matrices with larger T extents. Unfortunately we do not have good enough data to do a $T = \infty$ extrapolation with this set. This difference clearly shows the importance of taking into account the corrections due to finite T extent of the correlation matrices.

In [9] the energy difference between string states for SU(2) in three dimensions is also presented. Sophisticated wave functions and improved anisotropic gauge actions are used in that study. However they do not report taking the finite T corrections into account. They too see evidence of the energy difference crossing the π/r curve predicted by naive string theory and point to the possibility of the existence of a massive QCD string. Qualitatively, the degeneracy and level ordering of our uncorrected data is in agreement with that study at larger values of r and we believe that if that study is extended to larger physical T 's or the correction due to finite T extents is taken into account this crossing would not occur.

To look at the excited state in the $\{++\}$ channel, we formed the correlation matrix using different smearing parameters. In principle this matrix could be numerically diagonalised to obtain the eigenvalues and the energies once again obtained by taking the ratio of eigenvalues for different T 's. However diagonalisation of the correlation matrices showed that while the eigenvector corresponding to the ground state was stable, the eigenvector corresponding to the first excited state varied quite a bit for different values of T .

Since equation (20) assumes that the eigenvectors of both $C(T_1)$ and $C(T_2)$ are the same, we were unable to use this equation to extract the energies in this case. One way to force the eigenvectors to be equal is the diagonalise $C^{-1}(T_1)C(T_2)$, but even in this case it is not guaranteed that the eigenvectors are the same as we expect from the well determined single $C(T)$.

We therefore followed a different procedure for the E_1^{++} state. In this case, the correlation matrix was formed by using smeared sources as the basis states. Each element of this correlation matrix C can be expanded as [4]

$$C_{ij}(r, T) = \sum_{\alpha} \beta_i^{\alpha} \beta_j^{\alpha} e^{-E_{\alpha} T} \quad (26)$$

where $e^{-E_\alpha(r)T}$ is related to the eigenvalues of the transfer matrix and the product $\beta_i^\alpha \beta_j^\alpha$ is related to the overlap of the basis states between which this matrix element is taken. We truncated this expression at the second term and did a fit to a form $a_1 e^{-E_0 T} + a_2 e^{-E_1 T}$ (where $a_1 \equiv \beta_i^0 \beta_j^0$ and $a_2 \equiv \beta_i^1 \beta_j^1$) to extract E_0 and E_1 . The results are tabulated in table 7. The very nice agreement of the ground state energy assures us that the fit to E_1^{++} is reliable. Moreover since C was a 3×3 matrix, we did fits to several matrix elements to make sure that we obtained consistent values for the energy. Of course the coefficients a_1 and a_2 differed in each case.

Finally, in Fig. 8, we plot in a consolidated manner all the energy states at $\beta = 5$ for r values of 4,5,6,7 and 8. In this figure, the symbols $+$, \times , $*$ and

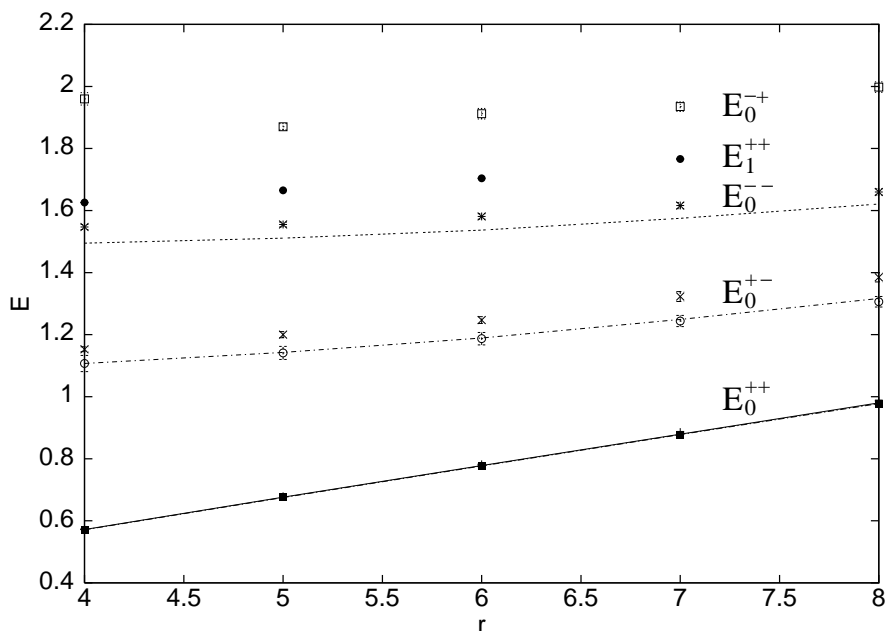


Fig. 8. The various energy states. Lattice size 24^3 . $\beta = 5$.

□ correspond to the naive ground state energies of the four different channels $\{++\}$, $\{+-\}$, $\{--\}$ and $\{-+\}$. The ■ corresponds to the ground state of the Polyakov loop and the line through it is the extrapolated ground state of the $\{++\}$ channel. The ○ corresponds to the corrected first excited state from the Polyakov loop and the line through that is the extrapolated ground

state in the $\{+-\}$ channel. The dashed line just below the $*$ indicates the extrapolated values in the $\{--\}$ channel. Finally the \bullet corresponds to the first excited state in the $\{++\}$ channel.

The difference between the various values for the ground state in the $\{++\}$ channel are not visible on this scale and in the figure only the \blacksquare is visible. However the split between the naive value and the extrapolated value is clearly visible in both the $\{+-\}$ and $\{--\}$ state. Our observation that the effect of extrapolation is higher for larger r is also evident here as the difference between the naive and the extrapolated values increase with increasing r .

We also want to point out that although the corrections due to finite volume and higher states are small effects, without taking them into account the excellent agreement we get between the Polyakov loop values and the extrapolated Wilson loop values would not occur.

Our results for the energies at $\beta = 7.5$ and $\beta = 10$ are given in tables 8 - 12.

6 Comparison at different β

To get some idea of how quantities depend on the lattice spacing, we look at the energy difference between the ground state and the first excited state. To compare the differences at different β 's we need to evaluate them at the same physical distance. We choose three such points, $1.05 r_0$, $1.2 r_0$ and $1.35 r_0$. Our results are contained in table 13.

In Fig. 9, the largest value of a^2 corresponds to $\beta = 5$, and is believed to lie slightly outside the scaling region for SU(2) lattice gauge theory in three dimensions. In the scaling region, according to the string prediction the energy differences should extrapolate to $\pi/1.05 = 2.992$, $\pi/1.2 = 2.618$ and $\pi/1.35 = 2.327$ respectively. Since the approach to continuum seems to be non-monotonic, we are presently unable do a reliable extrapolation to the continuum.

We also looked at the force and our findings are consistent with the expectation that the continuum limit is approached as $\mathcal{O}(a^2)$.

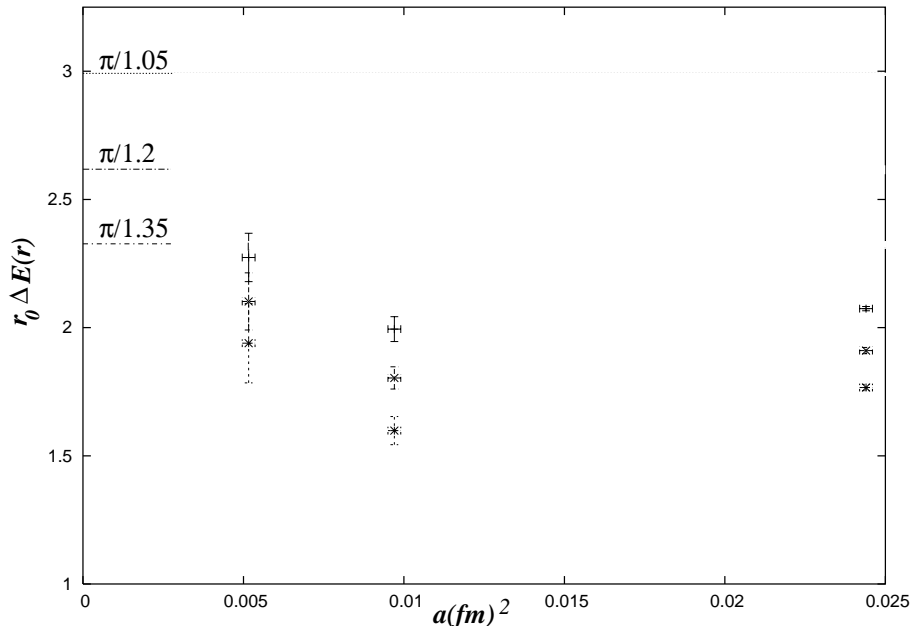


Fig. 9. The energy difference at different β .

7 Conclusion

In this work we have looked at the potentials and forces between infinitely heavy quarks and antiquarks and how they compare with predictions from the effective hadronic string picture.

Using the Lüscher - Weisz algorithm, we were able to go to previously inaccessible distances and for the first time we were able to systematically probe the exponentially small corrections due to finite T . Reasonably large values of T are required to see these effects and we were even able to extrapolate in some cases to infinite T . While these corrections are by themselves small, they are nevertheless absolutely crucial for comparing the data with the expected string spectrum.

Up to the distances we have measured, we have no reason to disbelieve the string prediction for the energy gap between the ground state and the first excited state. However it is necessary to use the extrapolated energy values to compute the difference. While the extrapolated data is not yet the

free string value (which is supposed to hold at large r), it seems to approach it. However the naive data actually crosses this value and shows a rise with r . This crossing and rise with r occurs at both $\beta = 5$ as well as 10. It is therefore very important to go to larger values of r to verify whether these trends continue.

As we have mentioned before, we have not used any of the existing sophisticated machinery for the wave functions but concentrated on the systematic corrections at larger T 's. The crucial point is that we have been able to take this correction into account order by order. We have only kept orders at which the corrections are larger than our statistical errors. Reasonably large values of T , allow us to see this effect on top of our statistical uncertainties. The Lüscher - Weisz algorithm lets us achieve this by making it possible to measure quantities accurately at the values of T we have used. However we expect that more accurate studies will require better wave functions as well, as the Lüscher - Weisz algorithm alone is not enough to reduce the fluctuation of the sources.

Finally it is clear that a more reliable continuum limit is necessary to confront the string predictions with lattice data and therefore studies at higher β have to be undertaken.

8 Acknowledgements

The author would like to express his deep gratitude to Peter Weisz for innumerable discussions and constant encouragement. Thanks are also due to Erhard Seiler, Ferenc Niedermayer, Philippe de Forcrand and Amol Dighe for several useful suggestions. Finally the computations were carried out at the theory cluster at Max-Planck-Institute Munich. The author is indebted to the institute for this facility.

A Error Analysis

We have two kinds of data. The directly measured quantities and the derived quantities. The directly measured quantities are the matrix elements obtained from measurement of the various Wilson loops and the Polyakov loop correlation functions. The derived quantities are the various energies

which are determined from the matrix elements. Below we outline how the errors were calculated in each case.

For all the Polyakov loop correlators and the ground states obtained from the different path combinations, the errors were calculated using the usual binned jackknife procedure. On the other hand, for the states in the same channel we used the naive errors since there was no bin size for which the errors on all the matrix elements were maximized. Also the naive and maximum errors differed only by about 15%.

Let us now come to the derived quantities. While calculating the errors on the forces and $c(r)$, it is possible to use the correlations between different values of r to ones advantage. To do so, $F(r)$ and $c(r)$ were calculated individually for each measurement and then we used the jackknife analysis on the various values of these quantities. However in this case too first we had to bin the data so that $F(r)$ and $c(r)$ determined from the bin averages satisfied all the known properties, which in this case are $c(r)$ being positive and $F(r)$ decrease with r as can be seen from the convexity of the potential [18] [23]. Finally there are the various fitted energy values. For the naive fits, the errors quoted are those calculated by the gnuplot fitting routine. For the extrapolated energies, these errors were unrealistically small and in those cases we used fits to “central value + error” to get an estimate of the errors on the fitted values.

References

- [1] J. Kogut and L. Susskind, Phys. Rev. D11 (1975) 395
- [2] G. S. Bali, Phys. Rep. 343 (2001) 1
- [3] M. Lüscher, K. Symanzik and P. Weisz, Nucl. Phys. B173 (1980) 365 ;
M. Lüscher, Nucl. Phys. B180 (1981) 317
- [4] L.A. Griffiths, C. Michael and P.E.L. Rakow, Phys. Lett. B129 (1983) 351
- [5] J. D. Stack, Phys. Rev. D27 (1983) 412; N. A. Campbell, C. Michael and P.E.L. Rakow, Phys. Lett. B139 (1984) 288; P. de Forcrand, G. Schierholz, H. Schneider and M. Teper, Phys. Lett. B160 (1985) 137; N.A. Campbell, A. Huntley and C. Michael, Nucl. Phys. B306 (1988) 51

- [6] M. Lüscher and P. Weisz, JHEP 0207 (2002) 049, hep-lat/0207003
- [7] M. Caselle, M. Hasenbusch and M. Panero, JHEP 0301 (2003) 057, hep-lat/0211012
- [8] K.J. Juge, J. Kuti and C.J. Morningstar, Nucl. Phys. Proc. Suppl. 73 (1999) 590, hep-lat/9809098; K. Jimmy Juge, Julius Kuti and C. Morningstar, hep-lat/0207004
- [9] K.J. Juge, J. Kuti and C.J. Morningstar, Contributed to 24th Johns Hopkins Workshop on Nonperturbative QFT Methods and Their Applications, hep-lat/0103008;
- [10] M. Lüscher and P. Weisz, JHEP 0109 (2001) 010, hep-lat/0108014
- [11] P. Majumdar, Contribution to 20th International Symposium on Lattice Field Theory, hep-lat/0208068
- [12] S. Kratochvila and P. de Forcrand, Contribution to 20th International Symposium on Lattice Field Theory, hep-lat/0209094
- [13] C. Alexandrou, P. de Forcrand and O. Jahn, Contribution to 20th International Symposium on Lattice Field Theory, hep-lat/0209062
- [14] H. B. Meyer, JHEP 0301 (2003) 048, hep-lat/0209145
- [15] C. Rebbi, Phys. Rep. 12 (1974) 1; J. Scherk, Rev. Mod. Phys. 47 (1975) 123
- [16] L. Brink and H. B. Nielsen, Phys. Lett. B45 (1973) 332
- [17] M. Lüscher, Comm. Math. Phys. 54 (1977) 283
- [18] C. Borgs and E. Seiler, Comm. Math. Phys. 91, (1983) 329
- [19] R. Sommer, Nucl. Phys. B411 (1994) 839, hep-lat/9310022
- [20] M. J. Teper, Phys. Rev. D59 (1999) 014512, hep-lat/9804008
- [21] Y. Schröder, Phys. Lett. B447 (1999) 321, hep-ph/9812205
- [22] M. Lüscher and U. Wolff, Nucl. Phys. B339 (1990) 222
- [23] C. Bachas, Phys. Rev. D33 (1986) 2723

$\beta = 5$			$\beta = 7.5$			$\beta = 10$		
r	$F(r)$	$c(r)$	r	$F(r)$	$c(r)$	r	$F(r)$	$c(r)$
3	0.1129 (2)	-0.1242 (8)	5	0.04350 (8)	-0.110 (21)	7	0.02318 (3)	-0.107 (1)
4	0.1062 (2)	-0.131 (2)	6	0.0421 (1)	-0.119 (30)	8	0.02266 (3)	-0.110 (1)
5	0.10320 (6)	-0.135 (1)	7	0.0412 (1)	-0.109 (16)	9	0.02224 (4)	-0.116 (2)
6	0.10167 (8)	-0.1345 (29)	8	0.0407 (2)	-0.107 (70)	10	0.02196 (4)	-0.118 (3)
7	0.10093 (9)	-0.133 (9)	9	0.0395 (11)	-	11	0.02175 (5)	-0.120 (4)
						14	0.02133 (5)	-0.119 (17)
						15	0.02125 (6)	-0.121 (27)

Table 2: $F(r)$ and $c(r)$ at different β and r . A ‘-’ indicates stable measurement was not possible.

β	lattice size	c	$a\sqrt{\sigma}$	r_0/a	$\sqrt{\sigma}r_0$
5.0	24^3	0.134	0.3124 (2)	3.94	1.231 (1)
7.5	36^3	0.117 (3)	0.1970 (2)	6.285	1.238 (1)
10.0	48^3	0.133 (4)	0.1437 (2)	8.58	1.233 (2)

Table 3: String tension and Sommer scale.

state	$r = 4$	$r = 5$	$r = 6$	$r = 7$	$r = 8$
E_0	0.5716 (2)	0.6755 (3)	0.7773 (3)	0.8778 (4)	0.9775 (5)
E_1	1.107 (26)	1.141 (21)	1.187 (20)	1.244 (18)	1.306 (17)

Table 4: Energies from Polyakov loop $\beta = 5$ Lattice 24^3 .

states	$r = 4$	$r = 5$	$r = 6$	$r = 7$	$r = 8$
E_0^{++}	0.5732 (5)	0.679 (1)	0.782 (1)	0.886 (2)	0.987 (2)
E_0^{+-}	1.153 (8)	1.20 (1)	1.247 (11)	1.323 (16)	1.385 (15)
E_0^{--}	1.547 (8)	1.555 (8)	1.581(9)	1.616 (10)	1.66 (1)
E_0^{-+}	1.96 (2)	1.87 (1)	1.912 (17)	1.935 (15)	1.998 (17)

Table 5: Naive Energies $\beta = 5$ Lattice 24^3

state	$r = 4$	$r = 5$	$r = 6$	$r = 7$	$r = 8$
E_0^{++}	0.57119 (5)	0.6751 (1)	0.7768 (1)	0.8777 (1)	0.9778 (1)
E_0^{*++}	0.5716 (1)	0.6757 (3)	0.7776 (5)	0.8784 (10)	0.9784 (16)
E_0^{+-}	1.1073 (18)	1.1429 (25)	1.1891 (20)	1.2492 (23)	1.3165 (22)
E_0^{--}	1.495 (7)	1.511 (6)	1.537 (7)	1.575 (7)	1.621 (7)

Table 6: Extrapolated energies. $\beta = 5$. Ground states in different channels

state	$r = 4$	$r = 5$	$r = 6$	$r = 7$	$r = 8$
E_0^{++}	0.5719 (1)	0.6761 (1)	0.7782 (2)	0.8792 (1)	0.9803 (3)
E_1^{++}	1.626 (31)	1.665 (20)	1.704 (33)	1.766 (6)	—

Table 7: Fitted Energies. $\beta = 5$. States in $\{++\}$.

state	$r = 6$	$r = 7$	$r = 8$	$r = 9$	$r = 10$
E_0^{++}	0.391 (3)	0.436 (5)	0.480 (6)	0.525 (7)	0.568 (8)
E_0^{+-}	0.871 (18)	0.903 (23)	0.918 (22)	0.963 (24)	0.984 (21)
E_0^{--}	1.171 (6)	1.159 (6)	1.161 (9)	1.167 (9)	1.181 (10)
E_0^{-+}	1.53 (2)	1.49 (2)	1.52 (2)	1.52 (2)	1.55 (2)

Table 8: Naive energies. $\beta = 7.5$. Ground states in different channels

state	$r = 6$	$r = 7$	$r = 8$	$r = 9$	$r = 10$
E_0^{++}	0.3825 (1)	0.4238 (2)	0.4642 (3)	0.5041 (3)	0.5435 (3)
E_0^{+-}	0.716 (9)	0.729 (7)	0.735 (7)	0.741 (11)	—

Table 9: Extrapolated energies. $\beta = 7.5$. Ground states in different channels

state	$r = 8$	$r = 9$	$r = 10$	$r = 11$	$r = 12$
E_0^{++}	0.308 (3)	0.335 (4)	0.360 (5)	0.387 (5)	0.412 (7)
E_0^{+-}	0.747 (28)	0.764 (31)	0.771 (29)	0.796 (32)	0.808 (31)
E_0^{--}	0.986 (20)	0.976 (19)	0.974 (20)	0.973 (20)	0.980 (20)
E_0^{-+}	1.354 (13)	1.331 (13)	1.344 (18)	1.344 (14)	1.369 (9)

Table 10: Naive energies. $\beta = 10$. Ground states in different channels using $T=2,4,6,8$

state	$r = 12$	$r = 13$	$r = 14$	$r = 15$	$r = 16$
E_0^{++}	0.3915 (6)	0.4154 (8)	0.4388 (9)	0.4629 (12)	0.4867 (16)
E_0^{+-}	0.663 (12)	0.681 (15)	0.694 (19)	0.719 (24)	0.733 (30)

Table 11: Naive energies. $\beta = 10$. Ground states in ++ and +- channels using T=4,8,12,16

state	$r = 8$	$r = 9$	$r = 10$	$r = 11$	$r = 12$
E_0^{++}	0.2961 (3)	0.31896 (39)	0.3419 (6)	0.36492 (77)	0.3869 (9)
E_0^{+-}	0.577 (7)	0.584 (11)	0.591 (12)	0.600 (16)	0.607 (19)

Table 12: Extrapolated energies. $\beta = 10$. Ground states in different channels

$r(r_0)$	$\beta = 5$	$\beta = 7.5$	$\beta = 10$
1.05 r_0	0.5264 (21)	0.3173 (77)	0.265 (11)
1.20 r_0	0.4849 (31)	0.287 (7)	0.245 (13)
1.35 r_0	0.4483 (31)	0.2543 (87)	0.226 (18)

Table 13: Comparison of the energy difference.